Deep Learning-based Link Configuration for Radar-aided Multiuser mmWave Vehicle-to-Infrastructure Communication

Andrew Graff, *Student Member, IEEE*, Yun Chen, *Student Member, IEEE*, Nuria González-Prelcic, *Senior Member, IEEE*, and Takayuki Shimizu

***Abstract*—Configuring millimeter wave links following a conventional beam training protocol, as the one proposed in the current cellular standard, introduces a large communication overhead, especially relevant in vehicular systems, where the channels are highly dynamic. In this paper, we propose the use of a passive radar array to sense automotive radar transmissions coming from multiple vehicles on the road, and a radar processing chain that provides information about a reduced set of candidate beams for the links between the road-infrastructure and each one of the vehicles. This prior information can be later leveraged by the beam training protocol to significantly reduce overhead. The radar processing chain estimates both the timing and chirp rates of the radar signals, isolates the individual signals by filtering out interfering radar chirps, and estimates the spatial covariance of each individual radar transmission. Then, a deep network is used to translate features of these radar spatial covariances into features of the communication spatial covariances, by learning the intricate mapping between radar and communication channels, in both line-of-sight and non-line-of-sight settings. The communication rates and outage probabilities of this approach are compared against exhaustive search and pure radar-aided beam training methods (without deep learning-based mapping), and evaluated on multi-user channels simulated by ray tracing. Results show that: (i) the proposed processing chain can reliably isolate the spatial covariances for individual radars, and (ii) the radar-to-communications translation strategy based on deep learning provides a significant improvement over pure radar-aided methods in both LOS and NLOS channels.**

***Index Terms*—Radar-aided mmmWave communication, vechicle-to-infrastructure (V2I), mmWave MIMO, automotive radar, deep learning-based link configuration, out-of-band information, beyond 5G, 6G.**

I. Introduction

THE automotive industry is incorporating advanced sensing and communication technologies to produce vehicles that are both more aware of their surroundings and able to communicate with others. This perceptual awareness has been achieved through the use of several onboard sensors, most notably automotive radars. The ability to communicate with infrastructure, referred to as vehicle-to-infrastructure (V2I) communication, allows for the sharing of sensor data, navigation information, multimedia, and more. These applications need high data rates to operate seamlessly.

Wireless communications at millimeter wave (mmWave) bands can achieve such high data rates. Communication at mmWave bands, however, typically requires gains through beamforming to reach acceptable signal-to-noise ratios (SNR), often requiring large antenna arrays. The configuration of these large arrays following standard beam training protocols introduces a large overhead (time required to configure the link). For example, for initial access (initial configuration of the link when the user enters the cell), when the number of antennas at the base station (BS) and the user are 64 and 16 respectively, and considering an analog MIMO architecture at both ends, the overhead of the beam training protocol associated to the 3GPP 5G NR standard varies in the range 750 ms to 5 s as a function of the number of synchronization blocks per burst [1]. This training overhead becomes even more demanding in multiuser V2I links, because the channel coherence times are short and users are rapidly entering and exiting the communication cell, resulting in a high probability that users are in initial access.

The onboard radars on many of these next-generation vehicles provide a unique signal of opportunity that contains out-of-band information that can be leveraged to reduce training overhead during initial access [2]. Since many automotive radars operate in a mmWave band adjacent to mmWave communications bands, the spatial covariance obtained at a passive radar receiver can be similar enough to the spatial covariance of the communication link, and therefore, it can be utilized to reduce the training overhead required to configure the link, as established in prior work [3].

This paper proposes the use of a roadside unit (RSU) equipped with a passive radar to aid in establishing multi-user (MU)-MIMO communication links at mmWave. The passive radar senses the transmitted frequency modulated continuous wave (FMCW) signals from multiple automotive radars at once, isolates the signal from each individual vehicle, estimates the spatial covariance of the individual FMCW signals, and then predicts the mmWave communication spatial covariance. This predicted communication covariance is then used to extract the main channel directions and select the beams that will act as analog precoders and combiners at the RSU, significantly reducing training overhead.

This material is based upon work partially supported by the National Science Foundation under Grant 2147955 and by a gift from Toyota.

A. Graff is with the Department of Electrical and Computer Engineering, The University of Texas at Austin, Austin, TX 78712, USA (e-mail: andrewgraff@utexas.edu).

Y. Chen and N. González-Prelcic are with the Department of Electrical and Computer Engineering, North Carolina State University, Raleigh, NC 27695, USA (e-mail: {ychen273,ngprelcic}@ncsu.edu).

T. Shimizu is with Toyota Motor North America, Mountain View, CA 94043 USA (e-mail: takayuki.shimizu@toyota.com).

A. Contributions

The main contributions of this paper are as follows:

- We propose to leverage the spatial covariance information obtained with a passive radar receiver at the RSU to configure the different mmWave communication links between the RSU and different vehicles in the road.
- We propose a passive radar processing chain that uses a filter bank architecture to isolate the individual FMCW signals from a reception containing multiple interfering FMCW signals from different vehicles. These isolated signals are then used to estimate the individual spatial covariances corresponding to the radar transmissions coming from different vehicles.
- We design multiple deep learning architectures to predict the communication spatial covariance from an estimated noisy radar spatial covariance. These neural networks learn the intricate relations and differences between the spatial covariances in the radar and communication bands. Three variations of neural networks are proposed to predict different functions useful for beamformer design: azimuth power spectrum (APS) prediction, eigenvector prediction, and covariance vector prediction.
- We create a ray tracing simulation of the radar-aided MU vehicular communication scenario to evaluate the performance of the proposed systems in terms of both the sum-rates and outage probabilities of different beam training strategies. This setup is consistent with the 3GPP V2X evaluation methodology for vehicular communication systems, and emulates the deployment of automotive radars in commercial vehicles. The obtained radar-communication channels dataset is made available to the research community to enable further work on radar-aided communication at mmWave [4].

B. Prior work

Out-of-band information to aid mmWave communication [2] can come from several sources, including sub-6 GHz systems [5]–[7], or sensors such as radar [3], [8]–[10], lidar [11], [12], inertial-measurement-units [13], [14], or position information [15]–[17].

Different approaches that exploit sub-6GHz signals have been proposed to reduce the beam training time or to estimate the spatial covariance, which is later used to design the beamformers. MmWave link configuration assisted by sub-6 GHz systems has, however, many limitations. The use of sub-6 GHz information in [5] is restricted to line-of-sight (LOS) channels. The strategies in [6], [7] are applicable to non-line-of-sight (NLOS) channels, but require that both the mmWave and sub-6 GHz channels have identical states (both LOS or both NLOS), which does not hold in general.

Position information extracted from a Global Positoning System (GPS) has also been used in different ways to reduce the overhead of mmWave link configuration. For example, inverse fingerprinting learns a subset of location-dependent beam-pairs based on past measurements in similar locations, such that with a high probability at least one of the vectors in the subset works well [18] [19] [20] [21]. A more sophisticated version of this idea exploits the sparsity of the MIMO channel to also provide beam recommendations in new positions where channel measurements are not available [17]. Further reductions in overhead can happen if there is also knowledge of other connected vehicles (which may have different sizes and act as blockages) [22] or other context [23] information. Beam-tracking for automotive vehicles aided by inertial-measurement-units (IMU) was proposed in [13], [14]. The common limitation of all these approaches is that they only target LOS scenarios.

A mmWave communication system aided by lidar is described in [11]. It considers two scenarios: the lidar is located at the base station (BS), or lidar data from two neighboring vehicles are fused. In [12], [24], different learning strategies predict V2I beam selections using precomputed spatial information collected from lidar sensors. The main limitation of these systems is that they are designed to operate only in LOS propagation.

The first work that proposed leveraging a radar sensor to aid millimeter wave link configuration considers an active radar at the RSU [8] to illuminate receivers on the vehicle and estimate the radar covariance. This is also the first study that experimentally shows there is a similarity between the angular information extracted from the radar and the communication spatial covariances, even when the center frequencies of operation are different. In [9], a dual function radar and communication system was proposed for simultaneously sensing vehicles and establishing the communication link aided by the sensing information. Position information obtained with a radar unit at the road infrastructure was also used in [25] to reduce the overhead of the beam training protocol. The accuracy of position information provided by radar is higher than that provided by GPS, which leads to a larger reduction in communication overhead when exploiting position information provided by a radar sensor than when leveraging GPS-based position, as shown in the field measurements provided in [26]. The high accuracy of radar locations was also exploited in [10] in the context of vehicle-to-vehicle (V2V) communication.

Although all these approaches based on an active radar provide an interesting reduction of the link configuration overhead, they only perform well in LOS scenarios. An additional limitation is that the allocation of power to active radar sensing may be prohibitive given a power budget at the roadside unit. Alternatively, a passive radar approach was taken in [3], where the RSU senses signals transmitted from automotive radars onboard the vehicles themselves. This solves the power consumption issue and allows NLOS estimation, but the study was restricted to a single-user case without interference from multiple radars. Furthermore, there is an inherent mismatch between the estimated radar covariance and the true communication covariance due to different operation frequencies or different locations of the radars and communication transceivers in the vehicles.

In this paper, we overcome these limitations by building upon our preliminary work in [27] to add multiuser capabilities and to further refine the covariance estimate by translating the radar covariance to the communication domain. To this aim, we use neural networks which effectively learn the mismatches between radar and communication channels. Although the

work in [27] already explores the idea of learning mismatches, only a single user scenario and the estimation of the APS are considered.

Notation: We use the following notation throughout the paper. Bold lowercase $\mathbf{x}$ is used for column vectors, bold uppercase $\mathbf{X}$ is used for matrices, non-bold letters x, X are used for scalars. $[\mathbf{x}]_i$ and $[\mathbf{X}]_{i,j}$, denote ith entry of $\mathbf{x}$ and entry at the ith row and jth column of $\mathbf{X}$, respectively. We use the serif font, e.g., x, for the frequency-domain variables. Superscript T, $*$ and $\dagger$ represent the transpose, conjugate transpose and pseudo inverse, respectively. $\mathbf{0}$ and $\mathbf{I}$ denote the zero vector and identity matrix respectively. $\mathcal{CN}(\mathbf{x}, \mathbf{X})$ denotes a complex circularly symmetric Gaussian random vector with mean $\mathbf{x}$ and covariance $\mathbf{X}$, and $\mathcal{U}[a, b]$ is a Uniform random variable with support $[a, b]$. We use $\mathbb{E}[\cdot]$ and $\|\cdot\|_{\mathrm{F}}$ to denote expectation and Frobenius norm, respectively.

II. System model

We consider the MU-MIMO V2I communication system represented in Fig. 1, where the RSU is located on the side of a roadway and U ego-vehicles are driving along the road with other non-connected vehicles. The RSU is equipped with a passive radar uniform linear array (ULA) and a communications ULA. Both the radar and the communication system operate at mmWave bands. The ego vehicles have 4 ULAs for communications and 4 single-antenna automotive radars. The communication arrays in the vehicles are placed in accordance with 3rd Generation Partnership Project (3GPP) proposals [28], and the radar arrays are placed at the 4 corners of the vehicle as in many commercial models. The passive radar array at the RSU will use receptions of the automotive radar signals to estimate the radar spatial covariances for each link. These covariances will then be used to configure the MU-MIMO mmWave communication link.

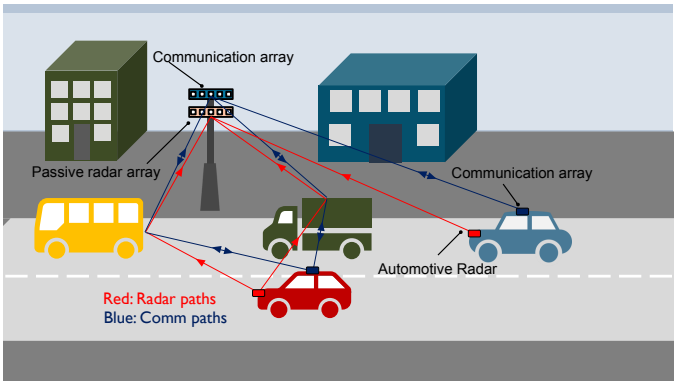

Fig. 1: A multiuser V2I communication system where the RSU is equipped with a communication array and a passive radar receiver, both operating at mmWave although in different bands. The radar array receives transmissions from the automotive radars (red), while the RSU and the vehicles transmit/receive data over the communication channel (blue). There is similarity between the radar and communication channels.

A. Communication system model

The communication array on the RSU is equipped with N_{RSU} antennas and $M_{\mathrm{RSU}} \leq N_{\mathrm{RSU}}$ RF-chains. We let A denote the number of communication arrays at the ego vehicle. Each vehicle array has N_{V} antenna elements and $M_{\mathrm{V}} \leq N_{\mathrm{V}}$ RF-chains. This hybrid architecture supports $N_{\mathrm{s}} \leq \min\{M_{\mathrm{RSU}}, M_{\mathrm{V}}\}$ data streams. The communication link is based on a K sub-carrier orthogonal frequency-division multiplexing (OFDM) system, with modulated symbols $\mathsf{s}[k] \in \mathbb{C}^{N_{\mathrm{s}} \times 1}$ such that $\mathbb{E}[\mathsf{s}[k]\mathsf{s}^*[k]] = \frac{P_{\mathrm{c}}}{KN_{\mathrm{s}}}\mathbf{I}_{N_{\mathrm{s}}}$ and P_{c} denotes the total average transmitted power. The baseband precoder $\mathbf{F}_{\mathrm{BB}}[k] \in \mathbb{C}^{M_{\mathrm{RSU}} \times N_{\mathrm{s}}}$ and RF precoder $\mathbf{F}_{\mathrm{RF}} \in \mathbb{C}^{N_{\mathrm{RSU}} \times M_{\mathrm{RSU}}}$ are combined to form the hybrid precoder $\mathbf{F}[k] = \mathbf{F}_{\mathrm{RF}}\mathbf{F}_{\mathrm{BB}}[k] \in \mathbb{C}^{N_{\mathrm{RSU}} \times N_{\mathrm{s}}}$ on sub-carrier k. The RF precoder is realized using quantized phase shifters and is the same across all subcarriers. Letting $\zeta_{i,j}$, $i = 1, \ldots, N_{\mathrm{RSU}}$, $j = 1, \ldots, M_{\mathrm{RSU}}$, be the quantized phase shift, the RF precoder is described as $[\mathbf{F}_{\mathrm{RF}}]_{i,j} = \frac{1}{\sqrt{N_{\mathrm{RSU}}}} e^{\mathrm{j}\zeta_{i,j}}$. The total power constraint is enforced as $\sum_{k=1}^{K} \|\mathbf{F}[k]\|_{\mathrm{F}}^2 = KN_{\mathrm{s}}$. The baseband combiner $\mathbf{W}_{\mathrm{BB}}^{(a)}[k] \in \mathbb{C}^{M_{\mathrm{V}} \times N_{\mathrm{s}}}$ and RF combiner $\mathbf{W}_{\mathrm{RF}}^{(a)} \in \mathbb{C}^{N_{\mathrm{V}} \times M_{\mathrm{V}}}$, $a = 1, \ldots, A$, are multiplied to form the hybrid combiner $\mathbf{W}^{(a)}[k] = \mathbf{W}_{\mathrm{RF}}^{(a)}\mathbf{W}_{\mathrm{BB}}^{(a)}[k] \in \mathbb{C}^{N_{\mathrm{V}} \times N_{\mathrm{s}}}$ on sub-carrier k. In the simulations we will assume that the number of streams and RF chains is equal to the number of vehicles supported by the RSU, and that the analog precoder/combiner corresponding to the link between the RSU and the uth vehicle is denoted as $[\mathbf{F}_{\mathrm{RF}}]_u$/$[\mathbf{W}_{\mathrm{RF}}]_u$, $u = 1, ..., U$.

The $N_{\mathrm{V}} \times N_{\mathrm{RSU}}$ frequency-domain MIMO channel at array $a \in A$ in vehicle u is denoted as $\mathbf{H}_u^{(a)}[k]$. Assuming perfect synchronization, the received signal on sub-carrier k after processing is

$$\mathbf{y}_u^{(a)}[k] = \mathbf{W}^{(a)_u *}[k]\mathbf{H}_u^{(a)}[k]\mathbf{F}[k]\mathbf{s}[k] + \mathbf{W}_u^{(a)*}[k]\mathbf{n}^{(a)}[k], \quad (1)$$

where $\mathbf{n}^{(a)} \sim \mathcal{CN}(\mathbf{0}, \sigma_{\mathbf{n}}^2\mathbf{I})$ is additive white Gaussian noise.

B. Channel model

The wideband channel is modeled geometrically with C clusters. Each of the clusters experiences a mean time delay $\tau_c \in \mathbb{R}$, mean angle-of-arrival (AoA) $\theta_c \in [0, 2\pi)$, and mean angle-of-departure (AoD) $\phi_c \in [0, 2\pi)$. Assuming there are R_c paths in each cluster, each path $r_c \in [R_c]$ has complex gain α_{r_c}, relative time-delay τ_{r_c}, relative arrival angle shift ϑ_{r_c}, and relative departure angle shift φ_{r_c}. The array response vectors are $\mathbf{a}_{\mathrm{RSU}}(\phi)$ at the RSU and $\mathbf{a}_{\mathrm{V}}(\theta)$ at the ego-vehicle. The uniform spacing between array elements is Δ, normalized to units of wavelength. The RSU response vector and ego-vehicle response vectors are defined as

$$\mathbf{a}_{\mathrm{RSU}}(\theta) = [1, e^{\mathrm{j}2\pi\Delta\sin(\theta)}, \cdots, e^{\mathrm{j}(N_{\mathrm{RSU}}-1)2\pi\Delta\sin(\theta)}]^{\mathsf{T}}. \quad (2)$$

$$\mathbf{a}_{\mathrm{V}}(\phi) = [1, e^{\mathrm{j}2\pi\Delta\sin(\phi)}, \cdots, e^{\mathrm{j}(N_{\mathrm{V}}-1)2\pi\Delta\sin(\phi)}]^{\mathsf{T}}. \quad (3)$$

Weremove the notation (a) in the channel $\mathbf{H}$ for the following equations. We define the analog filtering and pulse shaping effect at delay τ as $p(\tau)$. T_{c} denotes the signaling interval. The delay-d MIMO channel matrix $\mathbf{H}_u[d]$ is [29]

$$\mathbf{H}_u[d] = \sum_{c=1}^{C}\sum_{r_c=1}^{R_c} \alpha_{rc,u} p(dT_{\mathrm{c}} - \tau_{c,u} - \tau_{r_c,u}) \times \mathbf{a}_{\mathrm{V}}(\phi_{c,u} + \varphi_{r_c,u})\mathbf{a}_{\mathrm{RSU}}^*(\theta_{c,u} + \vartheta_{r_c,u}). \quad (4)$$

If there are D delay-taps in the channel, the channel at sub-carrier k, $\mathbf{H}[k]$ is [29]

$$\mathbf{H}_u[k] = \sum_{d=0}^{D-1} \mathbf{H}_u[d] e^{-\mathrm{j}\frac{2\pi k}{K} d}. \tag{5}$$

C. Covariance model

We define the spatial covariance at the RSU for the link with the uth vehicle on sub-carrier k as $\mathbf{R}_{\mathrm{RSU},u}[k] = \frac{1}{N_\mathrm{V}} \mathbb{E}[\mathbf{H}_u^*[k]\mathbf{H}_u[k]]$. By assuming that the covariance does not change across sub-carriers [30], we can create an estimate by averaging over all sub-carriers $\hat{\mathbf{R}}_{\mathrm{RSU},u} = \frac{1}{K}\sum_{k=1}^{K} \hat{\mathbf{R}}_{\mathrm{RSU},u}[k]$. As we will describe in Sec. II-E, our proposed system uses the covariance estimates to design the RF precoder at the RSU, while training symbols are used to design the baseband precoder, which can account for sub-carrier-dependent covariance variations [3] and multiuser interference.

D. Radar system model

Each automotive radar in the environment is assumed to operate in the mmWave band, transmiting a unique FMCW signal. We will assume there are M radars transmitting. The mth radar, for $m \in [M]$, has a chirp rate of β_m, a time offset of Δt_m, and a phase offset of $\Delta\phi_m$. We will assume all radars operate with the same bandwidth B. Then the chirp period is defined as $T_m = \frac{B}{\beta_m}$.

Then the transmitted signal can be defined as

$$s_m(t) = \sqrt{P_\mathrm{r}} \exp\left(j2\pi\left(f_r t + \frac{\beta_m t^2}{2}\right) + j\phi_m\right) \quad \text{for } t \in [\Delta t_m, \Delta t_m + T_m]. \tag{6}$$

This transmitted signal repeats every T_m seconds. The received signal on the N_r element antenna array on the RSU will be denoted as a vector $\mathbf{x}(t) \in \mathbb{C}^{N_\mathrm{r}}$. Assume that due to multipath effects, the radar transmission propagates along R_m paths. Each path $r_m \in [R_m]$ experiences an attenuation of α_{r_m} and a time delay of τ_{n,r_m} during propagation to the nth antenna. The received signal at antenna n is

$$[\mathbf{x}(t)]_n = \sum_{m=1}^{M}\sum_{r_m=1}^{R_m} \alpha_{r_m} s(t - \tau_{n,r_m}). \tag{7}$$

We can model the propagation delay as the sum of two components: one accounting for common distance τ and another accounting for the difference among antenna elements at the ULA τ'_n. This delay at antenna n is described as $\tau_{n,r_m} = \tau_{r_m} + \tau'_{n,r_m}$ [31]. We assume our ULA has half-wavelength spacing and that the signal from radar m and path r_m arrives at an angle of θ_{r_m}, so

$$\tau'_{n,r_m} = \frac{\sin\theta_{r_m}(n-1)}{2f_\mathrm{r}}. \tag{8}$$

Then we collect the I samples of the signal into a matrix $\mathbf{Y} \in \mathbb{C}^{N_\mathrm{r} \times I}$. Let $i \in \{1, 2, \cdots, I\}$ denote the sample index, and T_r denote the sampling time. Then the ith sample on the nth antenna is $[\mathbf{Y}]_{n,i} = [\mathbf{x}(iT_\mathrm{r})]_n$. The spatial covariance of the received radar signal could then be estimated as $\hat{\boldsymbol{R}} = \frac{1}{I}\mathbf{Y}\mathbf{Y}^*$.

However, this covariance estimate is not particularly useful when multiple vehicular radars are transmitting. The covariance will contain all of the interfering signals from all M vehicular radars that are transmitting. As a result, the azimuth power spectrum (APS) computed from such an estimate may be dominated by the contributions from higher SNR signals while the contributions from low SNR signals are undetectable due to the interference and sidelobes. A more useful covariance would be the isolated covariance of each transmitting radar signal. Let us define the true spatial covariance for signal m. This will be done by propagating a unit power Dirac-delta signal through the radar channel from radar m, i.e.

$$[\check{\mathbf{x}}_m(t)]_n = \sum_{r_m=1}^{R_m} \alpha_{r_m}\delta(t - \tau_{n,r_m}). \tag{9}$$

Then perform the same sampling and covariance estimation as before:

$$[\check{\mathbf{Y}}_m]_{n,i} = [\check{\mathbf{x}}_m(iT_\mathrm{r})]_n, \tag{10}$$

$$\boldsymbol{R}_m = \frac{1}{I}\check{\mathbf{Y}}_m\check{\mathbf{Y}}_m^*. \tag{11}$$

$\boldsymbol{R}_m$ is our ideal isolated spatial covariance from the radar signal m. Section III-A describes our designed signal processing chain that creates estimates $\hat{\boldsymbol{R}}_m$ of the isolated spatial covariance from the total received signal $\mathbf{x}(t)$.

For this paper, we assume that the communication links and automotive radars operate in separate bands where mutual interference between the two bands is negligible. This assumption is supported by the study in [32], which describes experimental results that show that the radar-to-communication interference can be neglected in this context.

E. Link configuration

We assume that the link configuration system at the RSU receives the estimated radar covariance for the link with each vehicle from the passive radar receiver. Then, an additional processing stage translates these estimated radar covariances into the averaged communication covariance $\hat{\mathbf{R}}_{\mathrm{RSU},u}$ for the link with the uth vehicle in initial access. Note that the radar and communication covariances are similar, but there are mismatches due to, for example, the different operation frequencies or different locations of the radar and communication antenna arrays. Section III-B includes our proposed solutions for this stage.

Once the estimate of the averaged communication covariance is available, the RF precoder phase shifts are configured based on a standard beam search over a restricted codebook. The subset of beams in this restricted codebook are selected as those around the direction of maximum power in the azimuth power spectrum (related to the communication covariance through the Fourier transform). The number of beams in the restricted codebook is a parameter of the system. The RF combiner is defined at the vehicle using a beam search over a full codebook. Note that overhead reduction in the beam training stage is achieved by the great reduction in the size of the restricted codebook used at the RSU.

To obtain the digital precoders and combiners after the RF stage has been designed, a practical system could use different

algorithms that can provide an estimation of the beamformed channel (propagation channel plus RF stage) based on the transmission of a sequence of training symbols. From the estimated channels, different state-of-the-art solutions for the frequency selective digital precoders and combiners are also available [33], [34]. In our simulations in Section IV, we show the performance of the analog counterpart of the proposed system, since our only goal is to show the effectiveness of the radar-aided beam training strategy (the innovation proposed in this work) independently of the approach for digital beamforming.

III. Radar-aided Multiuser Link Configuration

A. Multiuser Separation and Radar Covariance Estimation

As mentioned, the received signal $\mathbf{Y}$ contains contributions from all transmitting radars in the environment. However, the RSU must now attempt to estimate the individual radar covariances for each vehicle, which will later be used to assist in RF precoder design for downlink communications. We assume that for vehicles in initial access, the RSU has no knowledge of the automotive radar chirp rate or timing. Furthermore, the RSU may have no knowledge whether or not a new vehicle has entered its area-of-coverage and must be able to detect radar transmissions from new vehicles. As such, we propose a FMCW mixing filter bank processing chain to detect vehicles, suppress interference from other automotive radar signals, and estimate the spatial covariance for each vehicle in the area-of-coverage individually. The FMCW mixing filter bank correlates the received passive radar signals with several FMCW chirps, each with a different chirp rate. This correlation is effectively a matched filter, maximizing the output power of the correlator when the chirp rate of a received signal matches the chirp rate of the filter bank. Individual FMCW signals can be detected from the peaks of the filter bank correlator output. These detections provide an estimate of each FMCW signal's chirp rate and time-delay. With knowledge of the chirp rate and time-delay, the mixed signals corresponding to each detection can be multiplied by a time-delay correction signal, concentrating the power of the matched signal near DC. A lowpass filter is then applied, filtering out interference from other FMCW signals, thereby isolating the individual radar signals corresponding to each detection. These isolated signals are then used to estimate the spatial covariance of each detected radar.

For now, let's consider a single block within the mixing bank, which is visualized in Fig. 2. The received signal is mixed with a reference FMCW signal $s_{\text{ref}}(t)$ with the desired chirp rate β_{mix}. Much like the transmitted FMCW signals, the reference FMCW signal has a chirp period of T_{mix} and repeats every T_{mix} seconds,

$$s_{\text{ref}}(t) = \exp\left(-j2\pi\left(f_r t + \frac{\beta_r t^2}{2}\right)\right) \quad \text{for } t \in [0, T_m]. \tag{12}$$

The output mixed signal is denoted as $\mathbf{x}_{\text{mix}}(t)$, and can be written as

$$\mathbf{x}_{\text{mix}}(t) = \mathbf{x}(t) s_{\text{ref}}(t). \tag{13}$$

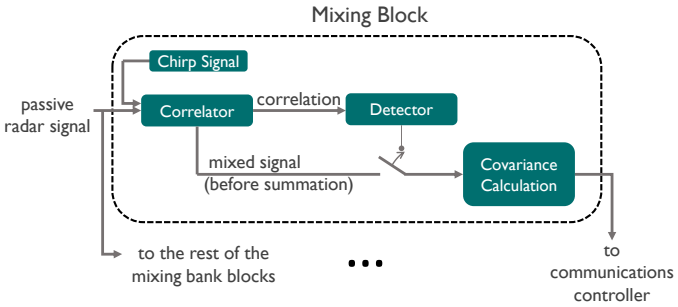

Fig. 2: Visualization of a single mixing block within the mixing bank. The received signal is mixed with a chirp signal, sampled, and correlated. The detector then determines whether a FMCW signal is present corresponding to the block's chirp rate and finds the chirp timing. The covariance is then estimated based on the mixed signal.

This signal after sampling is then called $\mathbf{Y}_{\text{mix}}$, and can be expressed as

$$[\mathbf{Y}_{\text{mix}}]_{n,i} = [\mathbf{x}_{\text{mix}}(iT_r)]_{n,i}. \tag{14}$$

Note that the received chirp signals are not time-aligned with the reference chirp signal. The output of this mixer is then sampled and processed digitally.

The next stage in the processing block is the correlator. The sampled signal is then digitally mixed with an offset-correction signal before the I samples are summed together. This digital mixing and summation is repeated for every lag. The output of the correlator is then passed to a detector. The digital correction signal for lag l is defined as

$$[S_{\text{corr}}]_{l,i} = exp\left(j2\pi\left(\frac{\beta_m (lT_r)^2}{2} iT_r\right)\right). \tag{15}$$

The corrected sampled mixed signal at lag l is defined as

$$[\mathbf{Y}_{\text{mix},l}]_{n,i} = ([\mathbf{Y}_{\text{mix}}]_{n,i})([S_{\text{corr}}]_{l,i}). \tag{16}$$

And finally, the correlator output is defined as

$$[\mathbf{C}]_{n,l} = \sum_{i=1}^{I} [\mathbf{Y}_{\text{mix},l}]_{n,i}. \tag{17}$$

The digital correction signal accounts for the frequency of the reference FMCW signal at the start of lag l. This makes the correlator output equivalent to mixing and summing with an FMCW signal that starts at frequency f_r at every lag l. This saves on hardware complexity by allowing each mixing block to only require mixing with a single FMCW reference signal. The digital correction is then an element-wise complex multiplication. Assuming that the FMCW reference signal is controlled by a voltage-controlled oscillator (VCO), the digital processor can have knowledge of the reference signals frequency at each sample time.

When the chirp start and chirp rate of the block align with the chirp start and chirp rate of a received signal, the magnitude of the output of the correlator will exhibit a sharp peak. For chirp rates that do not align, the output of the correlator will have its power spread out over the lag domain. To show this, consider a case where 51 mixing blocks are

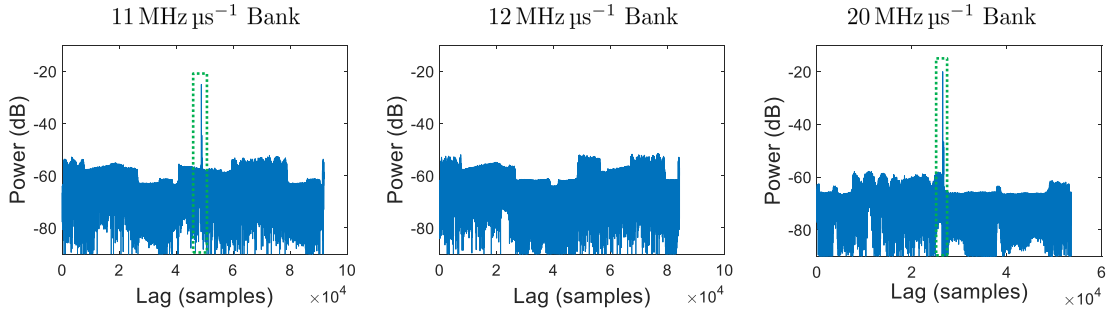

Fig. 3: The correlator output of 3 mixing blocks with reference FMCW chirp rates of 11, 12, and 19 MHz/μs. Sharp peaks are shown in the first and last output corresponding to passive radar receptions of signals with a matching chirp rate. The second output has no such peak.

used in the filter bank, each with a uniformly spaced chirp rate between 10 and 60 MHz/μs. This is visualized in Fig. 3, where the correlator output of the same received signals is shown for 3 of the 51 mixing blocks. In the 11 MHz/μs bank and 20 MHz/μs bank, sharp peaks exist because the received signal contains FMCW pulses matched to their mixing chirp rates of 11 and 20 MHz/μs. The 12 MHz/μs bank has no such peak, because the received signal contained no FMCW pulses with a chirp rate of 12 MHz/μs. In the 12 MHz/μs bank, the power of the chirp detected in the 11 MHz/μs bank becomes spread out over the lag domain. This spreading effects grow as the signal and mixing chirp rates become further separated. In the 20 MHz/μs bank, the chirp detected in the 11 MHz/μs bank is spread out significantly, allowing for the individual FMCW signal matching 20 MHz/μs to be detected. The remaining interference from the spread out signal is not present across the entire lag domain, however, so the detector of these peaks must be able to adapt to changing interference and noise levels. The objective of the detector is to determine whether such a peak exists in the output of the correlator and to remain robust

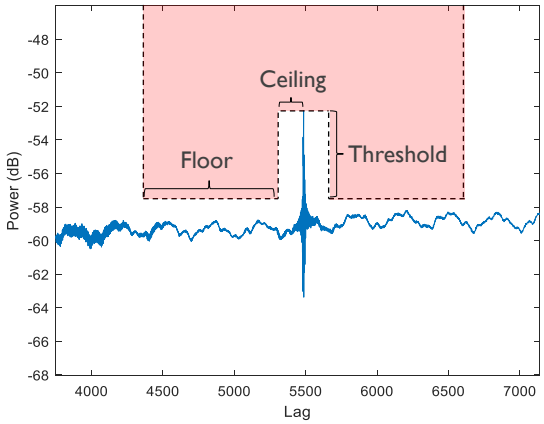

Fig. 4: A visualization of the max CFAR detector. For each lag, the boundary box defined by the guard cells and floor cells is defined relative to the power at the lag being tested. If the signal does not conflict with the boundary box, a detection is marked at that particular lag.

For our purposes, we propose the use of a max CFAR (constant false alarm rate) detector. The interference power at any given time delay and mixing block may not be known beforehand, especially as vehicles enter and exit the area-of-coverage. As such, an adaptive detection algorithm that estimates the interference power and determines a threshold dynamically is desirable. The max CFAR detector is visualized in Fig. 4. Max CFAR estimates the noise and interference power around a cell-under-test (CUT) by taking the maximum power of a set of cells that neighbor the CUT. A set of guard cells close to the CUT are ignored in this estimation, because power from the CUT may leak into close-by cells. However, we enforce that the power at the CUT is greater than all the powers in the guard cells. In our application, the set of guard cells must account for the delay spread of the radar channel. Once the noise and interference power has been estimated, a detection threshold is determined by multiplying the power by some scaling factor. This scaling factor can be tuned by the system designer to achieve a desired false alarm rate. If the power in the CUT exceeds this threshold, the system considers this a detection. Max CFAR can be implemented efficiently digitally with an FPGA (see [35] for example).

Let the N_{guard} be the number of guard cells, N_{floor} be the number of cells beyond the guard cells that are used to estimate the noise and interference power, and P_{det} be the power threshold for detection. Define the set of guard cell offsets as $\Delta L_{\text{guard}} = [-N_{\text{guard}}, 1] \bigcup [1, N_{\text{guard}}]$. Define the set of floor cell offsets as $\Delta L_{\text{floor}} = [-N_{\text{guard}} - N_{\text{floor}}, -N_{\text{guard}}] \bigcup [N_{\text{guard}}, N_{\text{guard}} + N_{\text{floor}}]$. Assume that the correlator output at lag l is our CUT. We decide to take the maximum power across antennas in these detection steps as well. The CUT power P_{CUT} is defined as

$$P_{\text{CUT}} = \max_n |[\mathbf{C}]_{n,l}|^2. \tag{18}$$

The noise and interference estimate is defined as

$$P_{\text{floor}} = \max_n \max_{\Delta l \in \Delta L_{\text{floor}}} |[\mathbf{C}]_{n,l+\Delta l}|^2. \tag{19}$$

The power in the guard cells is also defined as

$$P_{\text{guard}} = \max_n \max_{\Delta l \in \Delta L_{\text{guard}}} |[\mathbf{C}]_{n,l+\Delta l}|^2. \tag{20}$$

The CUT is then marked as a detection if the following

conditions are met:

$$\begin{aligned} P_{\text{CUT}} &> P_{\text{guard}}, \\ P_{\text{CUT}} &> P_{\text{det}} P_{\text{floor}}. \end{aligned} \tag{21}$$

Let D be the set of lags where detections are found. The sampled output of the mixer corresponding to these detected lags, $[\mathbf{Y}_{\text{mix},l}]_{n,i} \forall l \in D$, is passed to the covariance estimator. It should be clarified that the samples passed to the covariance estimator are samples before the summation operation in the correlator. By detecting the correct time delay and chirp rate of a particular FMCW reception and then mixing it with a reference chirp corresponding to these exact parameters, we experience a power gain in this particular FMCW signal and a suppression of the other interfering FMCW signals. Furthermore, this power is concentrated in spikes near DC since the correct lag and time delay have been estimated. Therefore, a lowpass filter with a bandwidth B_f greater than the multipath spread of the propagation channel can be applied to the detected signals to filter out the interfering radar transmissions.

$$\hat{\mathbf{Y}}_l = \text{lowpass}\{\mathbf{Y}_{\text{mix},l}\} \tag{22}$$

Assuming the detection is accurate, this process isolates the received FMCW signals from each vehicle, allowing the RSU to estimate each vehicle's radar spatial covariance separately. These spatial covariances are then subsequently passed to the communications controller, which will establish a link with the newly detected vehicles in the area-of-coverage.

B. Radar-to-Communication Covariance Mapping

The communications controller will now leverage the spatial covariance estimates collected from the passive radar to establish a communications link. While the radar channel and communications channels are not equivalent, the spatial covariances may be similar since both systems operate at mmWave and have receivers that are physically separated by a distance no greater than the size of the vehicle. To establish the communication link, a neural network will take the radar spatial covariance estimate and predict the communication link spatial covariance. The communications controller will then compute the direction of maximum power in the APS of this predicted covariance, select a restricted subset of beams from its codebook closest to this direction of maximum power, and then perform a standard beam search over this restricted codebook. The RF precoder phase shifts are configured to the communication controller's selection of beams from the codebook, and the baseband precoder can be configured using the training symbols. By restricting the codebook of the beam search, fewer training blocks need to be transmitted.

As per the previous section, the detector outputs a set of sampled post-mixing signals $[\mathbf{Y}_{\text{mix},l}]_{n,i} \forall l \in D$ that are filtered out to obtain $\hat{\mathbf{Y}}_l$. The radar spatial covariance can be estimated independently for each of these signals

$$\hat{\boldsymbol{R}}_l = \frac{1}{I} \hat{\mathbf{Y}}_l \hat{\mathbf{Y}}_l^*. \tag{23}$$

The filtering and mixing results in a large gain in the SIR, but some interference power may still remain. Assuming that detection l corresponds to the vehicle our system is establishing a communication link with, The controller must now estimate $\mathbf{R}_{\text{RSU}}$ from the noisy radar covariance estimate $\hat{\boldsymbol{R}}_l$. A neural network will be trained and applied to handle this mapping between the radar and communication domains. However, direct prediction of the complete covariance matrices ignores much of the spatial structure and requires unreasonably high dimensional inputs and outputs. Instead, we train neural networks to input and predict three lower-dimensional features related to the covariance: the APS, the dominant eigenvector, and the covariance vector, which is obtained as the first column of the covariance matrix.

A straightforward way to realize radar-to-communication mapping is to extract the APS from the radar and the communication covariance matrices using the DFT, and use them to train a neural network. Such a network, which predicts the communication APS using the radar APS as input, was described in the preliminary work [27]. Let $\boldsymbol{F}$ be a DFT matrix. The APS $\boldsymbol{d}$ of a spatial covariance matrix $\boldsymbol{R} \in \mathbb{R}^{N \times N}$ is defined as

$$\boldsymbol{d} = |\text{diag}\left(\boldsymbol{F}^* \boldsymbol{R} \boldsymbol{F}\right)|. \tag{24}$$

The directions of the beams formed by this APS are given in radians as $\theta_n = \arcsin\left(\frac{2n-N-1}{N}\right), \quad n = 1, ..., N$, assuming uniform $\lambda/2$ antenna spacing. In implementation, the radar APS will be computed and input into the trained neural network, which outputs a prediction of the communication APS. If the DFT beamforming matrix is not oversampled, this reduces the dimensionality of the neural network input and output from N^2 to N.

An alternative approach consists of using the dominant eigenvector of the estimated radar covariance to predict the dominant eigenvector of the communication covariance. Similar to APS prediction, it reduces the dimensionality of the neural network input and output from N^2 to N, simplifying the training and implementation of the neural network. Second, it can help further isolate the signal of interest from the remaining interference after isolation and filtering. In our communication protocol, which will be described in detail in Section IV-A, only a single stream will be transmitted to each target to ensure each link has the highest possible SNR. Therefore, predicting the dominant eigenvector of the communication covariance will naturally approximate the spatial weights corresponding to this stream. Consider the eigendecompositions $\hat{\boldsymbol{R}}_l = \mathbf{Q}_l \boldsymbol{\Lambda}_l \mathbf{Q}_l^{-1}$ and $\mathbf{R}_{\text{RSU}} = \mathbf{Q}_{\text{RSU}} \boldsymbol{\Lambda}_{\text{RSU}} \mathbf{Q}_{\text{RSU}}^{-1}$, where the columns of $\mathbf{Q}_l$ and $\mathbf{Q}_{\text{RSU}}$ are the eigenvectors of each covariance, and $\boldsymbol{\Lambda}_l$ and $\boldsymbol{\Lambda}_{\text{RSU}}$ are diagonal matrices containing the eigenvalues of each covariance. Let $\mathbf{v}_l$ be the eigenvector in $\mathbf{Q}_l$ corresponding to the greatest eigenvalue in $\boldsymbol{\Lambda}_l$. Let $\mathbf{v}_{\text{RSU}}$ be the eigenvector in $\mathbf{Q}_{\text{RSU}}$ corresponding to the greatest eigenvalue in $\boldsymbol{\Lambda}_{\text{RSU}}$. The neural network $\mathcal{N}_{\text{eig}}(\cdot)$ will take $\mathbf{v}_l$ as input and predict $\hat{\mathbf{v}}_{\text{RSU}}$. Just as the covariance has an APS, we can define the APS d of an eigenvector $\boldsymbol{v}$ as

$$\boldsymbol{d} = |\boldsymbol{F}^* \boldsymbol{v}|^2. \tag{25}$$

Finally, the third alternative relies on translating the radar covariance vector to the communication covariance vector [27]. In this alternative, the special structure of the covariance

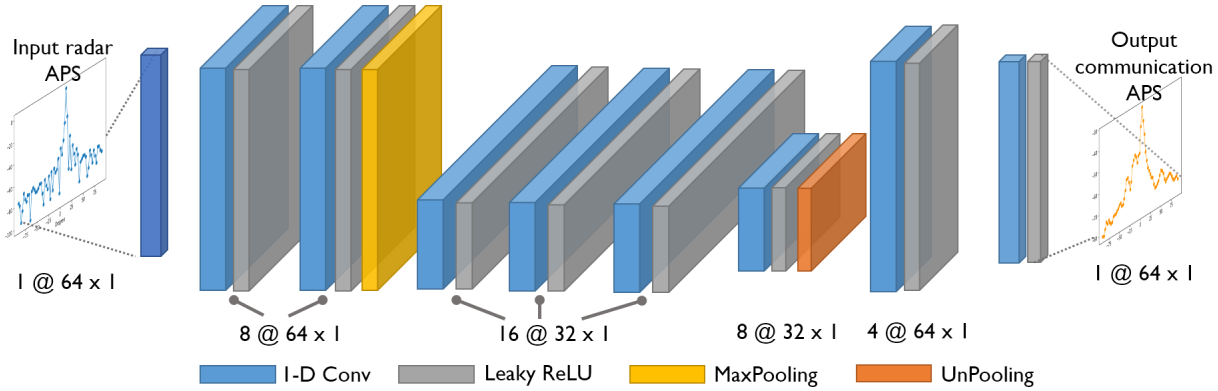

Fig. 5: The neural network architecture for APS predictions.

matrix is leveraged to reduce dimensionality. Toeplitz completion [3], [36] is first used to project the measured covariance matrix to the Toeplitz, Hermitian and positive semi-definite cone $\mathbf{T}_+^N$, i.e.,

$$\widetilde{\mathbf{R}}_l(\widetilde{\mathbf{R}}_{\text{RSU}}) = \arg\min_{\mathbf{X}\in\mathbf{T}_+^N} ||\mathbf{X} - [\hat{\mathbf{R}}_l(\widetilde{\mathbf{R}}_{\text{RSU}}) - \sigma_n^2\mathbf{I}]||_{\text{F}}, \quad (26)$$

where $\widetilde{\mathbf{R}}_l$ and $\widetilde{\mathbf{R}}_{\text{RSU}}$ are the projected covariance matrix for the radar and communication channels, which could be fully represented by their first columns, denoted as $\widetilde{\mathbf{r}}$ and called covariance vectors. This project the information of a covariance matrix a the closest Toeplitz matrix. Then, a neural trained to predict this communication cova the radar covariance vector. This method dimensionality of the neural network inpu N^2 to N.

C. Neural network architectures

Different network architectures are des tion for the 3 covariance features describe eigenvector, and covariance vector. Fig. 5 designed to predict the communication A APS. 1D convolutional layers are well-kn local features and are adopted in the propos LeakyReLU is used as the activation functio help avoid both dying ReLU and vanishing The loss function, which defines how error is penalized and how the gradients are dete mizing the network, is set as the MSE bet and true communication APS.

Fig. 6 illustrates the network design fo vector prediction. Unlike the APS networ prediction neural network has to handle complex data. The input to the network is a 64 element vector containing the complex values of the input eigenvector. This complex input vector is then converted from complex values to magnitude and phase components. The magnitude and phase components are then stacked together in a single vector of 128 elements. After this restructuring, the vectorized data passes through 5 fully-connected layers containing 128, 256, 512, 256, and 128 activation units each. Each activation unit uses a LeakyReLU activation function with a shape parameter of $\alpha = 0.1$. A dropout layer is also placed after the activations of the 3rd fully-connected layer, with a dropout rate of 50%. The output of the last layer is then scaled to unit norm before being output. The output data is a 128-element real-valued vector where the first 64 elements correspond to the real components of the predicted eigenvector and the last 64 elements correspond to the imaginary components of the predicted eigenvector. For optimizing this network, the loss function shown in Algorithm

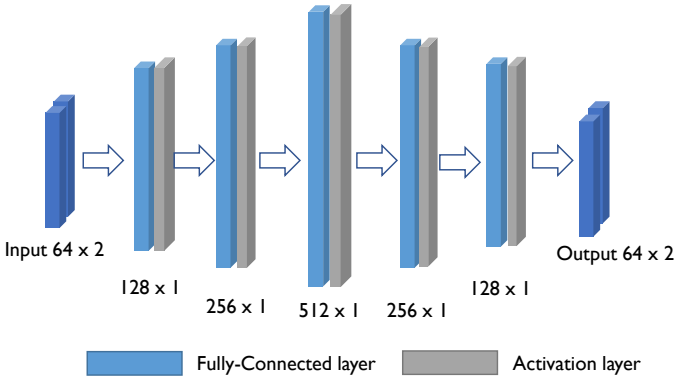

Fig. 6: The neural network architecture that is trained to predict communication link spatial eigenvectors from radar spatial eigenvector estimates.

The final network is designed for mapping the radar covariance vector to the communication covariance vector. $\widetilde{\mathbf{r}}_l$ and $\widetilde{\mathbf{r}}_{\text{RSU}}$ contain both real and imaginary parts, so the network should also take a two-channel input and output the predicted real and imaginary part of $\widetilde{\mathbf{r}}_{\text{RSU}}$, i.e.,

$$[\Re\{\hat{\mathbf{r}}_{\text{RSU}}\}, \Im\{\hat{\mathbf{r}}_{\text{RSU}}\}] = \mathcal{N}_{\text{col}}([\Re\{\widetilde{\mathbf{r}}_l\}, \Im\{\widetilde{\mathbf{r}}_l\}]; \mathbf{u}), \quad (27)$$

where $\mathbf{u}$ is the network parameter to be trained. As the covariance column is structure agnostic, and the real and imaginary parts are processed separately, special assumptions (e.g., the input follows any distributions or there are observable

Algorithm 1: APS Loss

Inputs:
$\boldsymbol{v}_{\text{pred}} \in \mathbb{C}^{N\times 1}$ - Predicted eigenvector
$\boldsymbol{v}_{\text{true}} \in \mathbb{C}^{N\times 1}$ - True eigenvector

Begin:
$\boldsymbol{c} \leftarrow$ chebwin(N,35)
$\boldsymbol{z}_{\text{pred}} \leftarrow |\text{FFT}(c \odot \boldsymbol{v}_{\text{pred}})|^2$
$\boldsymbol{z}_{\text{true}} \leftarrow |\text{FFT}(c \odot \boldsymbol{v}_{\text{true}})|^2$
loss $\leftarrow \frac{1}{N}\sum_{n=1}^{N} |[\boldsymbol{z}_{\text{pred}}]_n - [\boldsymbol{z}_{\text{true}}]_n|^2$
return loss

spatial features) are not necessary for the input. As such, layers that serve specific functions such as extracting local features or keeping historical memories are not used. Fully-connected layers, which allow learning from all the combinations of the features embedded in the covariance, are still suited for this situation. The network architecture used for eigenvector prediction is reused here with slight modifications. The middle layer containing 512 neurons is neglected, and dropout is not used as the network is not very deep. Here we use Tanh [37] to constrain the passing values to be in $[-1, 1]$. The predicted covariance vector is transformed back to the Toeplitz covariance matrix $\widetilde{\mathbf{R}}(\hat{\mathbf{r}}_{\text{RSU}})$, then the loss is calculated as

$$\mathcal{L}(\mathbf{u}) = \mathbb{E}\{||diag(\mathbf{F}^* \widetilde{\mathbf{R}}(\hat{\mathbf{r}}_{\text{RSU}})\mathbf{F}) - \mathbf{d}_c\}, \tag{28}$$

where $\mathbf{d}_c$ is the true communication APS.

IV. Simulation results

We will now present simulation data demonstrating the utility of multiuser covariance separation, machine-learning based covariance prediction, and our downlink MU-MIMO communication scheme using these new methods to reduce training overhead.

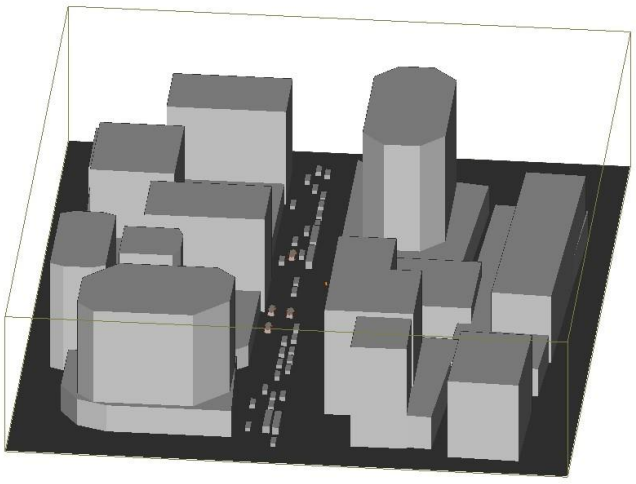

Fig. 7: The ray-tracing propagation environment. This models an urban roadway with 4 lanes.

A. Simulation setup

To generate our V2I communication and radar channels, ray-tracing simulations were conducted in Wireless Insite [38]. The simulated communication channels operate at 73 GHz and the simulated radar channels operate at 76 GHz. The ray-tracing environment models an urban roadway, which is visualized in Fig. 7. In this environment, a mix of medium and large buildings are located along both sides of the roadway. For simulation purposes, the material of the buildings is assumed to be concrete with a relative permittivity of 5.31, conductivity of $1.0509\,\text{S}\,\text{m}^{-1}$ in the communication band at $73\,\text{GHz}$, and a conductivity of $1.0858\,\text{S}\,\text{m}^{-1}$ in the radar band at $76\,\text{GHz}$ [39, Table 3]. The surface of the roadway is assumed to be asphalt that has a relative permittivity of 3.18, a conductivity of $0.4061\,\text{S}\,\text{m}^{-1}$ at $73\,\text{GHz}$, and a conductivity of $0.4227\,\text{S}\,\text{m}^{-1}$ at $76\,\text{GHz}$ [40]. Root-mean-square (RMS) surface roughness is also modeled as $0.2\,\text{mm}$ for concrete and $0.34\,\text{mm}$ for asphalt [40, Table 1]. In Wireless Insite, diffuse scattering is parameterized by a scattering coefficient in the range $[0, 1]$, which we select to be 0.4 for concrete and 0.5 for asphalt [41]. The fraction of diffuse reflections that experience cross-polarization is also parameterized with another coefficient in the range $[0, 0.5]$, which we select to be 0.5 for both concrete and asphalt. The material for the vehicles is assumed to be a perfect electric conductor metal.

The placement of the vehicles along the roadway is in accordance with option B for Urban scenarios as suggested by 3GPP [28, 6.1.2]. In this setup, we simulate 80% of vehicles being cars of size $5 \times 2 \times 1.6\text{m}$ and the remaining 20% of vehicles being trucks of size $13 \times 2.6 \times 3\text{m}$. We assume the speed of vehicles is dependent upon the lane they are positioned in, and that the spacing between vehicles is exponentially distributed with a mean dependent upon the vehicle speed. The speed of vehicles in each lane are 60, 50, 25, and $15\,\text{km}\,\text{h}^{-1}$, denoted s_l. For each vehicle, let $d_l \sim \text{Exp}(0.5/s_l)$. Then the distance from the previous vehicle is given by $\max(2, d_l)$ [28, 6.1.2]. Note that despite ascribing a velocity to each vehicle, each ray-tracing simulation operates in a static environment frozen in time. For each simulation, the type and placement of vehicles are generated randomly and independently according to the above distributions. After generating the vehicle placements, M cars are selected within the area-of-coverage to be active vehicles equipped with radar and communication arrays. In our simulations, $M = 4$ and the area-of-coverage is defined as the 60m section of roadway centered around the RSU.

The active cars are equipped with 4 communication arrays and 4 radar arrays. The communication arrays are placed at the front, sides, and rear of the car at a height of 1.6m. The radar arrays are placed at the 4 corners of the car with 10° rotation toward the front or rear of the car and a height of 0.75m. The antenna patterns for both the communication and radar antenna elements are chosen to have a half-power beamwidth of 120°. The arrays are assumed to be ULA with an inter-element spacing of half a wavelength. The radar and communication channels generated this way are available at [4].

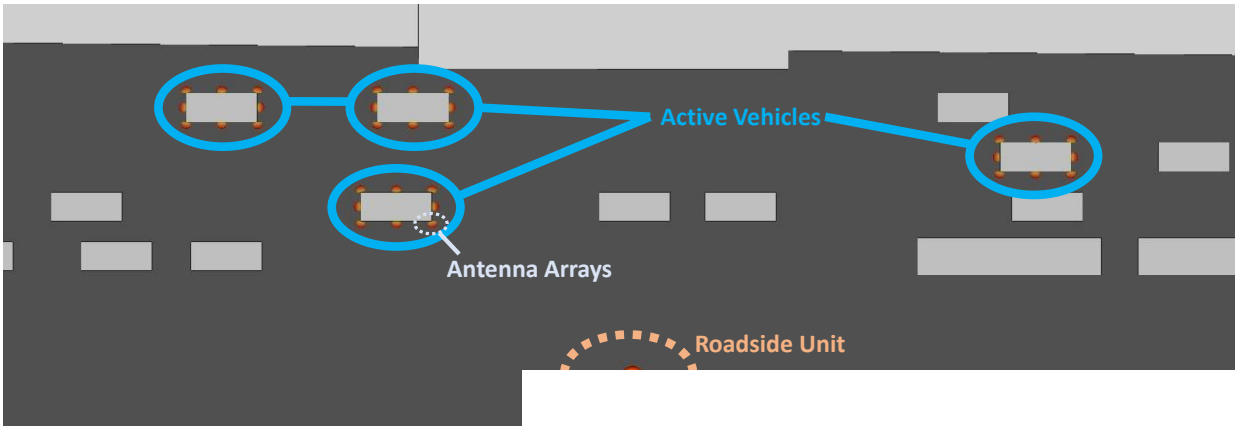

Fig. 8: An aerial view of the ray-tracing environment t with both radar and communication transceivers.

We simulate our communication link with a transmi of 24 dBm. We assume rectangular pulse-shaping f plicity. We use $K = 2048$ subcarriers with a su spacing of 240 kHz. $D = 512$ time-domain channel t used to capture the delay spread of the ray-traced ch Furthermore, a cyclic-prefix (CP) of $D-1$ samples is in in each OFDM symbol. At the RSU, the system has chains and 64 antenna elements. At the vehicle, the sys 1 RF-chain and 16 antenna elements per array. The de protocol is visualized in Fig. 9. This protocol is n after the standalone-downlink (SA-DL) scheme prop the beam management tutorial for 3GPP NR. In our p synchronization (SS) blocks are transmitted every coherence time. Each SS block spans 100% of the a subcarriers, uses 4 OFDM symbols, and supports u simultaneous beams in accordance with the number chains. Tracking (CSI-RS) blocks are transmitted per coherence time. Each CSI-RS block spans 25% available subcarriers, uses 1 OFDM symbol, and also s up to 4 simultaneous beams. All other resources not o with SS or CSI-RS blocks are used to transmit data to the UE vehicles. We will explore 3 different protocol variants for initial access: exhaustive search, assisted narrow search, and assisted wide search. The exhaustive variant requires all possible beam configurations to be searched over when establishing a link. This corresponds to a typical approach unaided by out-of-band or radar information. The assisted variants use either the direct radar covariance estimates or any of the three neural network predictions. In these assisted variants, the search space of beam configurations is reduced to a set of beams significantly smaller than the full codebook which the exhaustive search uses. Table I lists the number of RSU beams that are searched over for each variant, as well as the number of SS blocks required to search over that quantity of beams. This can be determined since each SS block supports 4 beams and the UE vehicle needs to search over 16 beams for every RSU. The narrow search only uses 4 beams, while the wide search uses 12 beams. For too small of a search size, the best beam may not be selected. For too large of a search size, the training overhead may become too costly and leave

Fig. 9: The downlink-based protocol. SS blocks use 100% of the subcarriers for training data. The CSI-RS blocks use 25% of the subcarriers for training data to track the channel.

TABLE I: Required search parameters for the three protocols.

Protocol	Beam Search Size	SS Blocks
Exhaustive Search	64	256
Assisted Narrow Search	4	16
Assisted Wide Search	12	48

The FMCW radars are capable of transmitting at chirp rates in the range $[10, 60]\text{MHz}\,\text{s}^{-1}$. Each vehicle independently selects a chirp rate $\beta \sim \mathcal{U}[10, 60]\text{MHz}\,\text{s}^{-1}$. Regardless of the chirp rate, each radar transmits an FMCW waveform with bandwidth of $B_r = 1\,\text{GHz}$ without downtime. The chirp period is defined as $T_p = \frac{B_r}{\beta}$. A random timing offset $\Delta t \sim \mathcal{U}[0, T_p]\text{s}$ is also selected for each vehicle. Each vehicle uses this chirp rate and timing offset for all 4 of its radars, assuming that all 4 radars transmit in a synchronized manner. An additional random phase offset $\epsilon \sim \mathcal{U}[0, 2\pi]$ is added to each transmitted radar signal.

B. *Neural network training*

A learning dataset was generated using the true covariances of the communication channels and the estimated radar covariances after detection and filtering. 3000 independent environments were generated, each with 4 covariance pairs

corresponding to the 4 active vehicles. This resulted in 12000 unique covariance training pairs. Of the 12000 pairs, 208 pairs were not detected from their radar transmissions and were discarded from the learning dataset, leaving 11792 properly detected pairs. This learning dataset was isolated and kept independent from the evaluation set used for the results shown later. The learning dataset was randomly sampled into a training dataset of 9434 entries and a validation dataset of 2358 entries. For each of the 3 neural networks, these covariances were pre-processed into APS's, dominant eigenvectors, and 1st columns of the covariance matrices.

The neural network was trained using the Adam optimizer. Early-stopping was used to halt training after a plateau of 16 training epochs and to restore the best weights that minimized the validation set. The learning rate was also halved after plateaus of 6 training epochs, down to a minimum learning rate of $1e-6$. The training was run using Tensorflow and accelerated using an Nvidia GTX 1060 GPU.

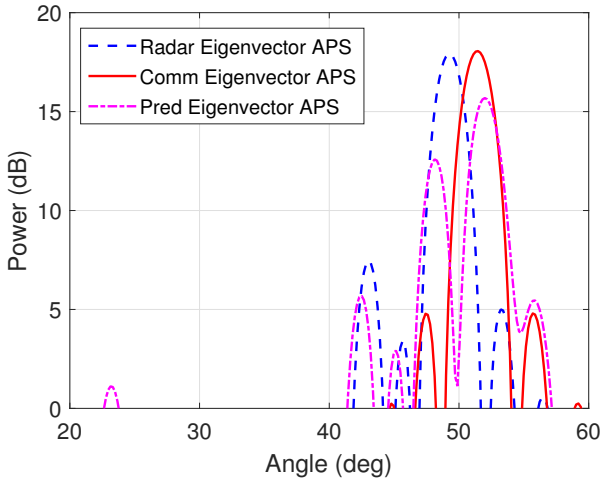

Fig. 10: An example of the trained network predicting an eigenvector input from the evaluation dataset. This example shows good alignment with the main beam of the communication APS and the predicted eigenvector's APS.

C. MmWave link configuration

Using the parameters above, we will now simulate the communication link in a Monte Carlo fashion to characterize the performance of the analog beamforming stage, and compare the three proposed network architectures for radar-to-communication mapping. 1000 independent environments were generated. For each environment, one active vehicle was selected at random to be in initial access, while the remaining three vehicles were selected to be in tracking. Channels were labeled as LOS if a direct path with zero reflections existed in the ray-tracing results. Otherwise, the channels were labeled as NLOS. Since the communication link operates in the band from 73 GHz to 74 GHz and the automotive radars operate in the band from 76 GHz to 77 GHz, we assume that spectral leakage is negligible.

As mentioned in Section IV-A, three beam training protocols were evaluated: exhaustive search, assisted narrow search,

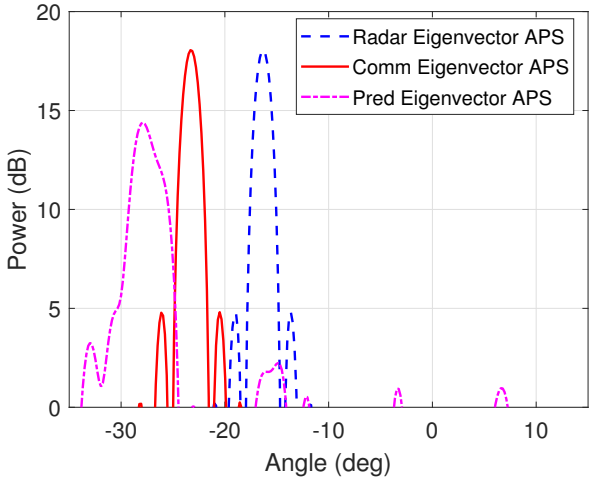

Fig. 11: A second example of the trained network predicting an eigenvector input from the evaluation dataset. This example shows a prediction where there is still some angular error between the peak of the predicted APS and the communication APS.

and assisted wide search. Each protocol defines a search space of beams which will be evaluated during the SS transmissions and requires a different number of SS blocks to be sent. Assume the RSU uses the same 2-bit DFT codebook for its $N_{\text{RSU}} = 64$ beams, and that the UE uses the same 2-bit DFT codebook for its $N_{\text{V}} = 16$ beams. Let $\mathcal{Q}(.)$ define the 2-bit quantization function. Then the RSU codebook $\mathbf{C}_{\text{RSU}}$ is defined as

$$[\mathbf{C}_{\text{RSU}}]_i = \mathcal{Q}\left(\frac{1}{N_{\text{RSU}}}\mathbf{a}_{\text{RSU}}\left(\arcsin\left(\frac{2i - N_{\text{RSU}} - 1}{N_{\text{RSU}}}\right)\right)\right) \quad \forall i \in [N_{\text{RSU}}]. \tag{29}$$

Similarly, the UE codebook $\mathbf{C}_{\text{V}}$ is defined as

$$[\mathbf{C}_{\text{V}}]_i = \mathcal{Q}\left(\frac{1}{N_{\text{V}}}\mathbf{a}_{\text{RSU}}\left(\arcsin\left(\frac{2i - N_{\text{V}} - 1}{N_{\text{V}}}\right)\right)\right) \quad \forall i \in [N_{\text{V}}]. \tag{30}$$

Let the beam search spaces for vehicle u be defined as a set $S_{\text{RSU},u}$ and $S_{\text{V},u}$. Then the best RF-precoder $\mathbf{f}_u$ and RF-combiner $\mathbf{w}_u$ are selected as

$$\{\mathbf{f}_u, \mathbf{w}_u\} = \arg \max_{\mathbf{f}_u \in S_{\text{RSU}}, \mathbf{w}_u \in S_{\text{V}}} \sum_{k=1}^{K} \log_2\left(1 + (\mathbf{w}_u^* \mathbf{H}_u[k]\mathbf{f}_u)^2\right). \tag{31}$$

We assume that the vehicles in tracking always select the best pair of RF-precoders and RF-combiners, so for those vehicles $S_{\text{RSU},u} = [N_{\text{RSU}}]$ and $S_{\text{V},u} = [N_{\text{V}}]$. Let the selected RF-precoders and RF-combiners be stacked into matrices such that $[\mathbf{F}_{\text{RF}}]_u = \mathbf{f}_u$ and $[\mathbf{W}_{\text{RF}}]_u = \mathbf{w}_u$. If we assume that $\mathbf{F}_{\text{BB}}[k]$ and $\mathbf{W}_{\text{BB}}[k]$ are diagonal matrices, then the signal power and interference power for the stream to UE u at subcarrier k can be defined as

$$P_{\text{sig},u}[k] = ([\mathbf{W}_{\text{RF}}]_u^* \mathbf{H}_u[k][\mathbf{F}_{\text{RF}}]_u)^2, \tag{32}$$

and

$$P_{\text{int},u}[k] = \sum_{l \neq u} ([\mathbf{W}_{\text{RF}}]_l^* \mathbf{H}_u[k][\mathbf{F}_{\text{RF}}]_l)^2. \quad (33)$$

Recall that we transmit each stream with a power of $P_t = 24$ dBm. With equal power allocation across all subcarriers, each subcarrier in each stream has a transmit power of $P_t = -9.1$ dBm. Assume a thermal noise of $N_0 = -174$ dBm/Hz, a system noise factor of 10dB, and a subcarrier spacing of $B_{\text{sc}} = 240$ MHz. Then the noise power per subcarrier is $P_n = -110.2$ dBm. The signal-to-interference-noise ratio (SINR) can be defined as

$$\text{SINR}_u[k] = \frac{P_{\text{sig},u}[k] P_t}{P_{\text{int},u}[k] P_t + P_n}. \quad (34)$$

After computing the SINR, the spectral efficiency can be defined as

$$s_u = \sum_{k=1}^{K} \log_2 (1 + \text{SINR}_u[k]). \quad (35)$$

Let T_{train} be the effective time spent transmitting training data from the SS and CSI-RS blocks. "Effective" refers to an average over all subcarriers. Let N_{SS} be the number of SS blocks and $N_{\text{CSI-RS}}$ be the number of CSI-RS blocks sent in the transmitted frame. Also let ν denote the fraction of subcarriers used by CSI-RS blocks. The effective training time is then computed as

$$T_{\text{train}} = T_{\text{sym}} \frac{N_{\text{SS}} N_{\text{sym-per-SS}} + \nu N_{\text{CSI-RS}} N_{\text{sym-per-CSI-RS}}}{N_{\text{beams}}}. \quad (36)$$

Now define T_{coh} as the channel coherence time and assume that the communication system repeats its training protocol every T_{coh} seconds. We can then compute the effective rate R_u for each link as

$$R_u = (1 - \frac{T_{\text{train}}}{T_{\text{coh}}}) B_{\text{sc}} s_u. \quad (37)$$

The sum-rate is then defined as

$$R_\Sigma = \sum_u R_u. \quad (38)$$

The sum-rate results are plotted in Fig. 12 for the assisted narrow search and Fig. 13 for the assisted wide search. Both plots include the exhaustive search results for comparison. Due to the large training overhead of the exhaustive search, the exhaustive strategy achieves poor sum-rates for short coherence times. Below 0.005 s, the exhaustive strategy requires more training symbols than what can be fit within one coherence interval, resulting in no data transmission. Comparatively, the assisted strategies allow the links to be established for even short coherence intervals. In Fig. 12, the assisted search based on covariance vector prediction achieves the highest rate for the entire range of coherence times, with the assisted search based on the eigenvector prediction slightly below. The pure radar-assisted search without learning based radar-to-communication mapping has similar performance at long coherence times, but the performance declines much faster at shorter times. The APS prediction neural network provides the lowest sum-rates of the assisted strategies at longer coherence

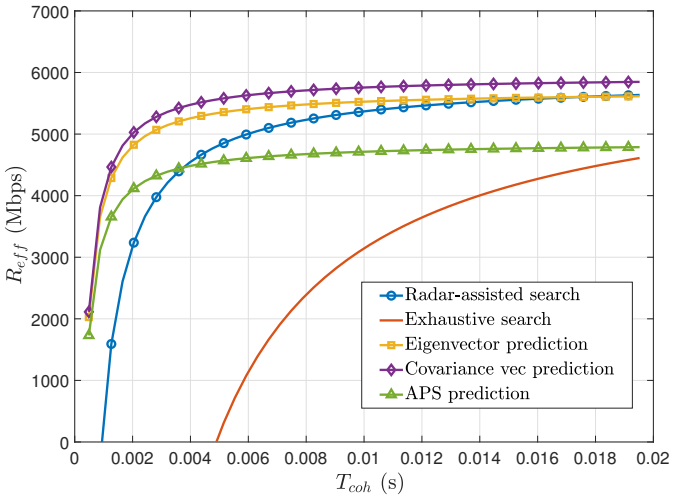

Fig. 12: The Monte Carlo sum rate results over all 4 users using an exhaustive search and all versions of the assisted narrow search.

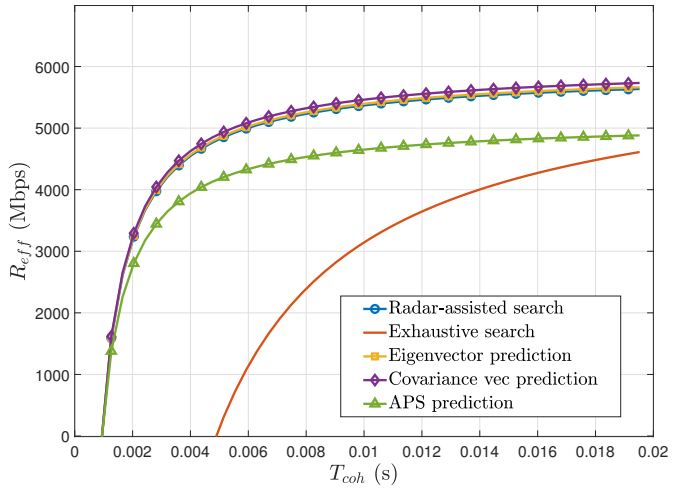

Fig. 13: The Monte Carlo sum rate results over all 4 users using an exhaustive search and all versions of the assisted wide search.

times, yet outperforms the radar-assisted search at very short coherence times. All of the assisted strategies show significant rate improvements over the exhaustive search, which is infeasible for short coherence times due to the large training overhead required. In Fig. 13, all the assisted methods use slightly more training overhead to reduce the likelihood that the optimal beam is missed. As a result, the difference in sum-rates between assisted strategies based on covariance vector prediction, eigenvector prediction, and pure radar-assisted is reduced.

D. Outage and Detection Errors

Our system can experience two main failures. The first is a failure to detect an FMCW signal that was transmitted. This will be called the probability of missed detection P_m. The second is failure to achieve a high enough SNR in the

communication link to transmit at a meaningful data rate. This will be called the probability of outage P_o. These metrics are evaluated on the vehicle in initial access for each simulation instance. Of the 1000 instances each with a single vehicle in initial access, the FMCW transmissions were not detected in 15 instances giving $P_m = 0.015$. Of the remaining 985 instances, the sum rate results were computed. Let us define the minimum supported rate as R_{min} and the index of the vehicle in initial access in instance i, out of N_i total instances, as u_i. The rate for this vehicle is R_{u_i}. Then the probability of outage is defined as

$$P_o = \frac{1}{N_i} \sum_{i=1}^{N_i} \mathbb{1}(R_{u_i} < R_{\text{min}}). \tag{39}$$

Set $R_{\text{min}} = 100\,\text{Mbps}$. Of the 985 instances with correct detection, 775 were classified as LOS and 210 were classified as NLOS. The assisted wide search (12 beams) was used for these results. The LOS probability of outage is shown in Fig. 14, and the NLOS probability of outage is shown in Fig. 15. As expected, the NLOS cases tend to have a higher probability of outage for all beam training methods. Below coherence times of $T_{coh} = 5\,\text{ms}$, the exhaustive search requires too many spectral resources to complete before the channel is incoherent, resulting in a probability of outage of 1. In both the LOS and NLOS cases, the covariance vector prediction neural network yields a reduction in the probability of outage compared to all other methods for coherence times below approximately 6 ms. Eigenvector prediction and pure radar-assisted strategies have roughly similar performance, while APS prediction has a notably higher outage probability in the same region. This demonstrates that our assisted strategies provide clear benefits over an exhaustive search in both LOS and NLOS propagation environments at short coherence times. Furthermore, learning-based assisted methods, especially the covariance vector prediction, can provide even further benefits compared to a pure radar-assisted search.

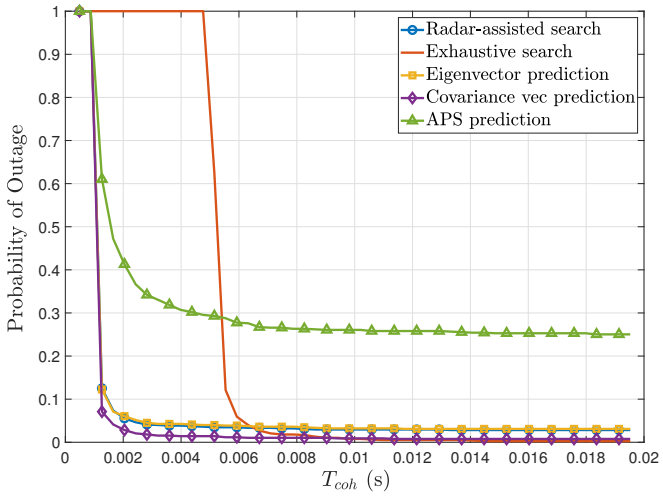

Fig. 14: The LOS probability of outage for the vehicle in initial access with an outage rate of $R_{\text{min}} = 100\,\text{Mbps}$.

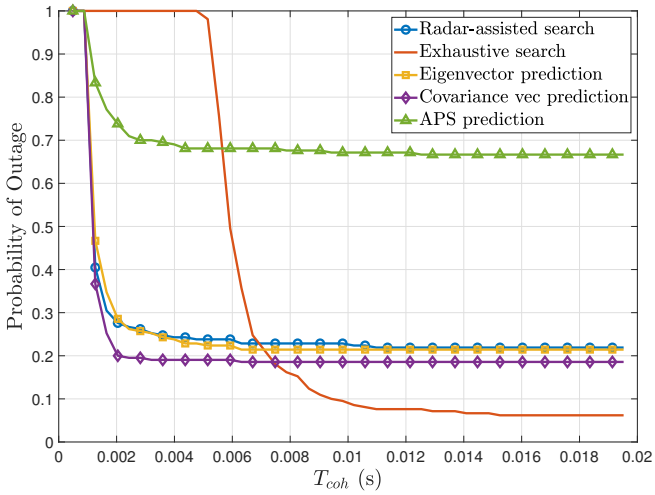

Fig. 15: The NLOS probability of outage for the vehicle in initial access with an outage rate of $R_{\text{min}} = 100\,\text{Mbps}$.

V. Conclusion and Future Work

In this work, we extended the application of radar-assisted beam training to multi-user communications. We designed a processing chain to estimate the individual spatial covariances of multiple interfering FMCW signals measured at a passive antenna array, and trained a neural network to predict selected features of the communication spatial covariances based on the estimated radar covariances. The proposed approaches were evaluated against a traditional exhaustive beam search strategy and an approach that used the APS of the estimated radar covariance without any further refinement based on a neural network. The features used for neural network prediction include the APS, the dominant eigenvector, and the covariance vector. Ray tracing software was used to generate mmWave radar and communication channels to create a training set for optimizing the neural network, and an evaluation dataset for comparing the beam training methods. The proposed assisted methods show drastic increases in the sum-rate compared to the exhaustive search. Our study additionally showed that the assisted search based on the learned covariance vector provides higher sum-rates and a lower probability of outage than all other assisted methods, in both LOS and NLOS environments.

These results show that out-of-band spatial information from passive radars can be used for multi-user systems when special processing is implemented to estimate signal parameters and filter out interference. In addition, the intricate differences between radar spatial characteristics and the communication channel spatial characteristics can be learned through deep learning, yielding more accurate channel predictions even in NLOS channels. This improved accuracy allows the system to reduce the size of its beam search, significantly reducing overhead and increasing the data rate.

Future work should explore the detection of automotive radars beyond FMCW, including OFDM and PMCW radar. On the communications side, addressing the problem of radar-aided beam reconfiguration, to track the variations of the vehicular channels after the link has been established, is also

an interesting area of research.

REFERENCES

[1] M. Giordani, M. Polese, A. Roy, D. Castor, and M. Zorzi, "A tutorial on beam management for 3gpp nr at mmwave frequencies," *IEEE Communications Surveys and Tutorials*, vol. 21, no. 1, pp. 173–196, 2019.

[2] N. González-Prelcic, A. Ali, V. Va, and R. W. Heath, "Millimeter-wave communication with out-of-band information," *IEEE Communications Magazine*, vol. 55, no. 12, pp. 140–146, 2017.

[3] A. Ali, N. González-Prelcic, and A. Ghosh, "Passive radar at the roadside unit to configure millimeter wave vehicle-to-infrastructure links," *IEEE Transactions on Vehicular Technology*, vol. 69, no. 12, pp. 14 903–14 917, 2020.

[4] WiSeCom Lab., "Radar-Comm. Channel Data Set," 2022. [Online]. Available: https://github.com/WiSeCom-Lab/DL-based-radar-aided-mmWave-V2X

[5] M. Hashemi, C. E. Koksal, and N. B. Shroff, "Out-of-band millimeter wave beamforming and communications to achieve low latency and high energy efficiency in 5G systems," *IEEE Transactions on Communications*, vol. 66, no. 2, pp. 875–888, 2018.

[6] A. Ali, N. González-Prelcic, and R. W. Heath, "Millimeter wave beam-selection using out-of-band spatial information," *IEEE Transactions on Wireless Communications*, vol. 17, no. 2, pp. 1038–1052, 2018.

[7] ——, "Spatial covariance estimation for millimeter wave hybrid systems using out-of-band information," *IEEE Transactions on Wireless Communications*, vol. 18, no. 12, pp. 5471–5485, 2019.

[8] N. González-Prelcic, R. Méndez-Rial, and R. W. Heath, "Radar aided beam alignment in mmWave V2I communications supporting antenna diversity," in *2016 Information Theory and Applications Workshop (ITA)*, 2016, pp. 1–7.

[9] F. Liu, W. Yuan, C. Masouros, and J. Yuan, "Radar-assisted predictive beamforming for vehicular links: communication served by sensing," *IEEE Transactions on Wireless Communications*, vol. 19, no. 11, pp. 7704–7719, 2020.

[10] C. Aydogdu, F. Liu, C. Masouros, H. Wymeersch, and M. Rydström, "Distributed radar-aided vehicle-to-vehicle communication," in *2020 IEEE Radar Conference (RadarConf20)*, 2020, pp. 1–6.

[11] A. Klautau, N. González-Prelcic, and R. W. Heath, "LIDAR data for deep learning-based mmWave beam-selection," *IEEE Wireless Communications Letters*, vol. 8, no. 3, pp. 909–912, 2019.

[12] T. Woodford, X. Zhang, E. Chai, K. Sundaresan, and A. Khojastepour, "Spacebeam: Lidar-driven one-shot mmwave beam management," in *Proceedings of the 19th Annual International Conference on Mobile Systems, Applications, and Services*, ser. MobiSys '21. New York, NY, USA: Association for Computing Machinery, 2021, p. 389–401. [Online]. Available: https://doi.org/10.1145/3458864.3466864

[13] M. Brambilla, M. Nicoli, S. Savaresi, and U. Spagnolini, "Inertial sensor aided mmWave beam tracking to support cooperative autonomous driving," in *2019 IEEE International Conference on Communications Workshops (ICC Workshops)*, 2019, pp. 1–6.

[14] A. Ali, J. Mo, B. L. Ng, V. Va, and J. C. Zhang, "Orientation-assisted beam management for beyond 5g systems," *IEEE Access*, vol. 9, pp. 51 832–51 846, 2021.

[15] P. Kela, M. Costa, J. Turkka, M. Koivisto, J. Werner, A. Hakkarainen, M. Valkama, R. Jantti, and K. Leppanen, "Location based beamforming in 5G ultra-dense networks," in *2016 IEEE 84th Vehicular Technology Conference (VTC-Fall)*, 2016, pp. 1–7.

[16] W. Miao, C. Luo, G. Min, L. Wu, T. Zhao, and Y. Mi, "Position-based beamforming design for UAV communications in LTE networks," in *ICC 2019 - 2019 IEEE International Conference on Communications (ICC)*, 2019, pp. 1–6.

[17] T.-H. Chou, N. Michelusi, D. J. Love, and J. V. Krogmeier, "Fast position-aided mimo beam training via noisy tensor completion," *IEEE Journal of Selected Topics in Signal Processing*, vol. 15, no. 3, pp. 774–788, 2021.

[18] V. Va, T. Shimizu, G. Bansal, and R. W. Heath, "Position-aided millimeter wave V2I beam alignment: a learning-to-rank approach," in *2017 IEEE 28th Annual International Symposium on Personal, Indoor, and Mobile Radio Communications (PIMRC)*, Oct. 2017, pp. 1–5.

[19] V. Va, J. Choi, T. Shimizu, G. Bansal, and R. W. Heath, "Inverse multipath fingerprinting for millimeter wave V2I beam alignment," *IEEE Transactions on Vehicular Technology*, vol. 67, no. 5, pp. 4042–4058, May 2018.

[20] V. Va, T. Shimizu, G. Bansal, and R. W. Heath, "Online learning for position-aided millimeter wave beam training," *IEEE Access*, vol. 7, pp. 30 507–30 526, 2019.

[21] K. Satyanarayana, M. El-Hajjar, A. A. M. Mourad, and L. Hanzo, "Deep learning aided fingerprint-based beam alignment for mmWave vehicular communication," *IEEE Transactions on Vehicular Technology*, vol. 68, no. 11, pp. 10 858–10 871, Nov. 2019.

[22] Y. Wang, A. Klautau, M. Ribero, A. C. K. Soong, and R. W. Heath, "MmWave vehicular beam selection with situational awareness using machine learning," *IEEE Access*, vol. 7, pp. 87 479–87 493, 2019.

[23] G. H. Sim, S. Klos, A. Asadi, A. Klein, and M. Hollick, "An online context-aware machine learning algorithm for 5G mmWave vehicular communications," *IEEE/ACM Transactions on Networking*, vol. 26, no. 6, pp. 2487–2500, 2018.

[24] M. B. Mashhadi, M. Jankowski, T.-Y. Tung, S. Kobus, and D. Gündüz, "Federated mmwave beam selection utilizing lidar data," *IEEE Wireless Communications Letters*, vol. 10, no. 10, pp. 2269–2273, 2021.

[25] A. Ali, N. González-Prelcic, and A. Ghosh, "Millimeter wave V2I beam-training using base-station mounted radar," in *2019 IEEE Radar Conference (RadarConf)*, 2019, pp. 1–5.

[26] A. Graff, A. Ali, and N. González-Prelcic, "Measuring radar and communication congruence at millimeter wave frequencies," in *53rd Asilomar Conference on Signals, Systems, and Computers*, 2019, pp. 925–929.

[27] Y. Chen, A. Graff, N. González-Prelcic, and T. Shimizu, "Radar aided mmWave vehicle-to-infrastructure link configuration using deep learning," in *IEEE Global Communications Conference*, 2021.

[28] 3GPP, "Study on evaluation methodology of new vehicle-to-everything (V2X) use cases for LTE and NR," 3rd Generation Partnership Project (3GPP), TR 37.885, Sep. 2018, version 15.1.0. [Online]. Available: http://www.3gpp.org/DynaReport/37885.htm

[29] A. Alkhateeb and R. W. Heath Jr., "Frequency selective hybrid precoding for limited feedback millimeter wave systems," vol. 64, no. 5, pp. 1801–1818, May 2016.

[30] E. Bjornson, D. Hammarwall, and B. Ottersten, "Exploiting quantized channel norm feedback through conditional statistics in arbitrarily correlated MIMO systems," vol. 57, no. 10, pp. 4027–4041, 2009.

[31] V. Katkovnik, M.-S. Lee, and Y.-H. Kim, "High-resolution signal processing for a switch antenna array FMCW radar with a single channel receiver," 2002, pp. 543–547.

[32] A. Graff, A. Ali, N. González-Prelcic, and A. Ghosh, "Automotive radar and mmwave mimo v2x communications: Interference or fruitful coexistence?" in *2020 IEEE Radar Conference (RadarConf20)*, 2020, pp. 1–5.

[33] A. Alkhateeb and R. W. Heath, "Frequency selective hybrid precoding for limited feedback millimeter wave systems," *IEEE Transactions on Communications*, vol. 64, no. 5, pp. 1801–1818, 2016.

[34] J. P. González-Coma, J. Rodríguez-Fernández, N. González-Prelcic, L. Castedo, and R. W. Heath, "Channel estimation and hybrid precoding for frequency selective multiuser mmwave mimo systems," *IEEE Journal of Selected Topics in Signal Processing*, vol. 12, no. 2, pp. 353–367, 2018.

[35] R. Cumplido, C. Torres, and S. Lopez, "On the implementation of an efficient FPGA-based CFAR processor for target detection," in *(ICEEE). 1st International Conference on Electrical and Electronics Engineering, 2004.*, 2004, pp. 214–218.

[36] N. J. Higham, "Computing the nearest correlation matrix—a problem from finance," *IMA journal of Numerical Analysis*, vol. 22, no. 3, pp. 329–343, 2002.

[37] B. L. Kalman and S. C. Kwasny, "Why tanh: choosing a sigmoidal function," in *[Proceedings 1992] IJCNN International Joint Conference on Neural Networks*, vol. 4. IEEE, 1992, pp. 578–581.

[38] "Wireless Insite," http://www.remcom.com/wireless-insite.

[39] I. T. U. (ITU), "Effects of building materials and structures on radiowave propagation above about 100 MHz," Tech. Rep. ITU-R P.2040-1, Jul. 2015.

[40] E. S. Li and K. Sarabandi, "Low grazing incidence millimeter-wave scattering models and measurements for various road surfaces," vol. 47, no. 5, pp. 851–861, 1999.

[41] Remcom, "5G mmwave channel modeling with diffuse scattering in an office environment." [Online]. Available: https://www.remcom.com/examples/2017/6/22/5g-mmwave-channel-modeling-with-diffuse-scattering-in-an-office-environment

Andrew M. Graff received the B.S. and M.S. degrees in electrical and computer engineering from The University of Texas at Austin, Austin, TX, USA, in 2019 and 2022 respectively. He is currently working toward the Ph.D. degree at the Department of Electrical and Computer Engineering at the University of Texas at Austin. He is currently a Graduate Research Assistant with the UT Radionavigation Lab, University of Texas at Austin. His research interests include estimation theory, wireless signal processing, array processing, and secure and robust sensing. Mr. Graff was a recipient of the 2020 Qualcomm Innovation Fellowship.

Yun Chen received her B.S degree in information engineering from Southeast University, Nanjing, China, in 2017, and her M.S. degree in electrical and computer engineering from The University of Texas at Austin, Austin, TX, USA, in 2020. She is currently a PhD student associated with Wireless Sensing and Communication Lab at NC State University. Her interest lies in the integration of communication and sensing with machine learning (deep learning) in mmWave vehicular networks, specifically in developing advanced algorithms that enhance the localization precision and reliability in V2X communication systems. She held research internship positions at Ericsson, Santa Clara, CA, USA in 2019 and 2020, and at Qualcomm, San Diego, CA, USA, in 2021 and 2022. She won the best paper award in IEEE Wireless Communications and Networking Conference 2020, and she received Summer Graduate Fellowship of the College of Engineering at NCSU in May, 2022.

Nuria González-Prelcic received her Ph.D. in Electrical Engineering in 2000 from the University of Vigo, Spain. She joined the faculty at NC State as an Associate Professor in 2020. She was previously an Associate Professor in the Signal Theory and Communications Department at the University of Vigo, Spain, and also held visiting positions at the University of Texas at Austin and the University of New Mexico. She was also the founding director of the Atlantic Research Center for Information and Communication Technologies (atlanTTic) at the University of Vigo (2008-2017). She is an Editor for IEEE Transactions on Communications. She is an elected member of the IEEE Sensor Array and Multichannel Technical Committee and the IEEE Signal Processing for Communications and Networking Technical Committee. She is a member of the IEEE SPS Integrated Sensing and Communication Technical Working Group. Her main research interests include signal processing theory and signal processing and machine learning for wireless communications: filter banks, compressive sampling and estimation, multicarrier modulation, massive MIMO, MIMO processing for millimeter-wave communication, including vehicle-to-everything (V2X), air-to-everything (A2X) and LEO satellite communication. She is also interested in joint localization and communication, joint radar and communication, and sensor assisted communication. She has published around 150 papers in the topic of signal processing for millimeter-wave communications, including a highly cited tutorial published in the IEEE Journal of Selected Topics in Signal Processing which has received the 2020 IEEE SPS Donald G. Fink Overview Paper Award and an article pioneering the idea of using mmWave WiFi signals for automotive radar that won the IEEE Vehicular Technology Society 2022 Best Vehicular Electronics Paper Award.

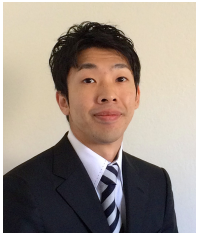

Takayuki Shimizu (S'09–M'12) received the B.E., M.E., and Ph.D. degrees from Doshisha University, Kyoto, Japan, in 2007, 2009, and 2012, respectively, where he studied physical-layer security exploiting multipath fading randomness in wireless communications. From 2009 to 2010, he was a Visiting Researcher at Stanford University, CA, USA. From 2012 to 2019, he worked at TOYOTA InfoTechnology Center, U.S.A., Inc. Currently, he is a Senior Principal Researcher at Toyota Motor North America, Inc., R&D InfoTech Labs, where he works on the research and standardization of wireless vehicular communications. His current research interests include millimeter-wave vehicular communications, vehicular communications for cooperative automated driving, and LTE/5G for vehicular applications. He is a 3GPP delegate for V2X standardization and a member of several SAE Technical Committees for V2X. He was a Workshop Co-Chair for the 2018 Fall IEEE Vehicular Technology Conference. He is a member of the IEICE. He received the 2010 TELECOM System Technology Award for Student from the Telecommunications Advancement Foundation and the 2020 IEEE Vehicular Networking Conference Best Paper Award.